Biophysical Journal
Article

Biophysical Society

The Amphipathic GM1 Molecule Stabilizes Amyloid Aggregates, Preventing their Cytotoxicity

Monica Bucciantini,[1,*] Manuela Leri,[1,2] Massimo Stefani,[1] Ronald Melki,[3] Sandra Zecchi-Orlandini,[4] and Daniele Nosi[4]

[1]Department of Experimental and Clinical Biomedical Sciences "Mario Serio," University of Florence, Florence, Italy; [2]Department of Neuroscience, Psychology, Area of Medicine and Health of the Child of the University of Florence, Florence, Italy; [3]Institut Francois Jacob, CEA and Laboratory of Neurodegenerative Diseases, CNRS 92265, Fontenay-Aux-Roses, France; and [4]Department of Experimental and Clinical Medicine, University of Florence, Florence, Italy

ABSTRACT Amyloid aggregates have been demonstrated to exert cytotoxic effects in several diseases. It is widely accepted that the complex and fascinating aggregation pathway involves a series of steps during which many heterogeneous intermediates are generated. This process may be greatly potentiated by the presence of amphipathic components of plasma membrane because they may serve as interaction, condensation, and nucleation points. However, there are few data regarding structural alterations induced by the binding between the amyloid fibrils and membrane components and its direct effects on cell integrity. In this study, we found, by 1-anilinonaphthalene 8-sulfonic acid and transmission electron microscopy/fast Fourier transform, that yeast prion Sup35 oligomers showed higher structural uniformity and altered surface properties when grown in the presence of monosialotetrahexosylganglioside, a component of the cell membrane. 3-(4,5-dimethylthiazol-2-yl)-2,5-diphenyltetrazolium bromide and confocal/sensitized Förster resonance energy transfer analyses revealed that these fibrils showed low cytotoxicity and affinity to plasma membrane. Moreover, time-lapse analysis of Sup35 oligomer fibrillation on cells suggested that the amyloid aggregation process per se exerts cytotoxic effects through the interaction of amyloid intermediates with plasma membrane components. These data provide, to our knowledge, new insights to understand the mechanism of amyloid growth and cytotoxicity in the pathogenesis of amyloid diseases.

SIGNIFICANCE Protein self-assembly in amyloid fibrils is involved in pathogenesis of a number of fatal diseases. Lipid membranes mediate this process, although the mutual influences between protein aggregation and membranes are unclear. In this study, we investigated the effects of nonspecific interactions between a ganglioside of plasma membrane, monosialotetrahexosylganglioside, and amyloid species obtained by a yeast protein model, Sup35, in terms of structural features and cytotoxicity. Our work demonstrates a self-assembly behavior of Sup35 in the presence of monosialotetrahexosylganglioside that leads to amyloid species with high structural uniformity and low cytotoxicity and affinity to cell membrane. Moreover, this study suggests that the amyloid aggregation process per se exerts cytotoxic effects through the interaction of amyloid intermediates with cell membrane.

INTRODUCTION

The term amyloidosis describes a wide group of pathologies occurring in various tissues and characterized by the presence of proteinaceous deposits grown from different peptides and proteins yet sharing the same basic cross-β structure. Diverse amyloid species produce pathological effects depending upon their cytotoxicity, which results from the selective interaction of the aggregates with biological structures of different complexity, from the organ to the cell level. For example, osteoarticular pathologies result from the presence of amyloid deposits in the skeletal system (1), whereas cell damage arises primarily from the molecular interaction of the aggregates with the plasma membrane (2–4). Amyloid aggregates are frequently found external to the cell membrane and may interact with a wide variety of molecules composing the extracellular matrix, membrane lipid, or protein molecules (5–8). The membrane as a whole and molecules sprouting from the cell membrane may act as a reactor, allowing monomeric or oligomeric peptides to interact and favoring their aggregation (9,10). Further data indicate surface interaction among monomeric or

Submitted July 10, 2019, and accepted for publication June 2, 2020.

*Correspondence: monica.bucciantini@unifi.it

Editor: Michael Brown.

https://doi.org/10.1016/j.bpj.2020.06.005

oligomeric species on cell surfaces as a triggering event enhancing membrane permeabilization, which eventually leads to cell dysfunction and death (11,12).

In this context, the importance of lipid composition and physicochemical properties of the cell membrane raised increasing attention (13), and it is known that cytotoxicity of in vitro grown amyloid aggregates results from their interplay with membrane lipid components (14).

It is reasonable to assume that the structural changes in the aggregation pattern of amyloid peptides, as well as the structural features of the final products deriving from the aggregation path on the cell surface, may be shaped by the interaction between intermediate species and plasma membrane components. It is well known that the amphipathic structure of amyloidogenic peptides may favor their aggregation and, possibly, their interaction with different molecules to gain structural stability. Therefore, the cytotoxic properties of fibrillar assemblies may differ on the basis not only of their structural features but also of the physicochemical properties of the interacting molecules. In fact, the interaction with hydrophobic low molecular weight synthetic or natural molecules, such as plant polyphenols, may stabilize intermediate or fibrillar products, reducing their ability to interact with the cell membrane and thus their toxicity (15). Moreover, various amphipathic molecules have been shown to modulate amyloid fibrillation by interacting with the aggregating peptides and proteins (16). Finally, hydrophilic compounds may also interfere with the aggregation path, as is the case of the charged calbindin, capable of retarding the growth of amyloid fibrils from the amyloid-β_{1-42} (Aβ_{1-42}) peptide (17). Amyloid assembly interactors in the highly dynamic cellular membrane gather numerous membrane channels and receptors, including the receptor for advanced glycation endproducts (RAGE), α-amino-3-hydroxy-5-methyl-4-isoxazolepropionic acid, N-methyl-D-aspartate, and insulin-like growth factor 1 receptors. Many of these components have been reported to interact with amyloid aggregates and have been implicated in amyloidosis (12,18–21). Actually, the consequences at the cell level of the interaction between the different amyloid intermediates and charged membrane components are poorly understood. This study aims at contributing to fill this gap by investigating, both in vitro and in vivo, the interaction occurring between a model of amyloid-forming polypeptide, the yeast translation termination factor Sup35, and the monosialotetrahexosylganglioside (GM1) during the aggregation process. GM1 is a known amyloid assembly interactor on plasma membrane (22,23). It has been demonstrated that cytotoxic effects may be elicited by GM1 interaction with fibrillar (2,24,25) as well as oligomeric (26–31) amyloid species. However, GM1 plays key functional roles at neuron membranes: protecting them against H_2O_2 and Aβ_{2535} toxicity via the activation of the Na^+,K+-ATPase in PC12 cells (32). Moreover, its expression is significantly reduced in transgenic animal models of Huntington's disease and in fibroblasts from Huntington's disease patients (33).

Sup35, which is not comparable with any amyloid disease in vertebrates, aggregates into fibrillar assemblies associated with the appearance of a heritable phenotypic trait in yeast: the [PSI+] prion phenotype (34,35). No endogenous proteins homologous to Sup35 are expressed in mammalian cells. Thus, Sup35 allows investigating the nonspecific mechanisms of amyloid assemblies binding to membrane lipids, such as GM1, and subsequent cytotoxicity. We used three-dimensional and sensitized Förster resonance energy transfer (FRET) confocal analyses carried out on murine endothelioma cell line (H-END) cells exposed to oligomers or fibrils of the yeast prion Sup35 grown in the absence or in the presence of mixed lipid membranes enriched in GM1. The effects of GM1 on Sup35 aggregation path and on the structural features of the resulting aggregates was evaluated by spectroscopy and transmission electron microscopy (TEM) implemented with fast Fourier transform (FFT) analysis. Fourier transform (FT) represents a useful mathematical tool in signal processing and analysis. When the FT operator is applied to image analysis, any feature of the image intensity distribution in the "real space" (x and y) is converted into a point in a "spatial frequency space" ("frequency" and "angle"). The position and the value of each point in spatial frequency space are related to the period and orientation of an image trait and its amplitude, respectively; FT represents, therefore, a tool suitable to disclose underlying periodic structural features (36,37).

MATERIAL AND METHODS

Preparation of phospholipid unilamellar vesicles

1,2-Dioleoyl-*sn*-glycero-3-phosphocholine (DOPC), brain sphingomyelin (BSM), cholesterol (Chol), and GM1 were purchased from Avanti Polar Lipids (Alabaster, AL) and used without further purification; BODIPY FL C5-GM1 was purchased from Thermo Fisher Scientific (Waltham, MA). Lipid vesicles were prepared by the lipid film hydration method, followed by extrusion; cholesterol, sphingomyelin, and phospholipid were independently dissolved in chloroform to a final concentration of 1 mg/mL. Large unilamellar vesicles (LUVs) were obtained by mixing appropriate amounts of single-lipid solutions with the starting molar composition DOPC/BSM/Chol (50:30:20 mol/mol/mol) and dried in glass tubes (8 mm in diameter) under a gentle nitrogen stream in a fume hood. GM1 or BODIPY FL C5-GM1 was substituted for BSM in proportions from 1 to 10 mol % (DOPC/BSM/GM1/Chol 50:29:1:20 and 50:20:10:20 mol/mol/mol/mol). The samples were resuspended in Sup35 assembly buffer (20 mM Tris-HCl buffer (pH 8.0), 200 mM NaCl, 5.0% v/v glycerol, 5.0 mM β-mercaptoethanol, 10 mM $MgCl_2$) and incubated for 1 h at room temperature to allow lipid hydration and vesicle formation, vortexing occasionally. After 1 h, the lipid suspensions were vigorously vortexed to allow complete detachment of hydrated lipids. The resulting suspension was subjected to five freeze-thaw cycles of 2 min each: freezing in dry ice, followed by 2 min thawing at 37°C. Then, the samples were sonicated for 20 min at 20 kHz on ice and subjected to extrusion through membranes with a 100-nm pore diameter using a Lipex Extruder (Transferra Nanosciences, Burnaby, Canada) to obtain a clear suspension of large unilamellar vesicles. The large lipid aggregates and titanium impurities coming from the sonicator probe

were removed by centrifuging the preparation for 10 min at 10,000 × *g*. Before each experiment, the size distribution of the vesicle population was checked using dynamic light scattering (Zetasizer Nano S; Malvern Instruments, Malvern, UK) and was shown to consist of a distribution centered at a diameter of 100 nm.

Assembly of Sup35 into fibrils

Sup35 is composed of three distinct regions: N, M, and C. The region C contains highly conserved GTP-binding consensus sites, binds Sup45, and provides the essential termination function of Sup35. M is highly charged, and positive lysines are concentrated in its N-terminal region, whereas negative glutamates are predominant in its C-terminal region and form a large negative charged patch on the protein surface (38). The function of M is unclear, although it appears to interact with Sup45. N is extremely rich in glutamine and asparagine (51 of 123 amino acids) and contains several imperfect repeats of the nonapeptide PQGGYQQYN. Sup35's isoelectric point is 7.0. Sup35 was expressed in *Escherichia coli*, purified as previously described (39) and stored as monomer at −80°C in a storage buffer (20 mM Tris-HCl buffer (pH 8.0), 1.0 M NaCl, 5.0 mM β-mercaptoethanol, 5.0% v/v glycerol).

Spontaneous fibrillation started after 24 h of dialysis of the protein sample against the assembly buffer (20 mM Tris-HCl buffer (pH 8.0), 200 mM NaCl, 5.0% v/v glycerol, 5.0 mM β-mercaptoethanol, 10 mM $MgCl_2$), differing from the storage one by a fivefold lower concentration of NaCl. Dialysis was followed by centrifugation at 18,500 × *g* for 10 min. Fibrillar samples were obtained after incubation for 72 h at 4°C with gentle agitation, at 10 μM final protein concentration, alone, in the presence of 10 μM of sialic acids (the negatively charged extracellular moiety of GM1; Sup35-SA-Fs), or in the presence of one of the following lipid dispersions:

- Sup35: DOPC/BSM/Chol (50:30:20 mol/mol/mol) 1:10 molar ratio (Sup35-Fs).
- Sup35: DOPC/BSM/GM1/Chol 50:29:1:20 mol/mol/mol/mol) 1:10 molar ratio; protein:GM1 1:0.1 (1:0.1 Sup35-GM1-Fs).
- Sup35: DOPC/BSM/GM1/Chol 50:20:10:20 mol/mol/mol/mol) 1:10 molar ratio; protein:GM1 1:1 (1:1 Sup35-GM1-Fs).
- Sup35: DOPC/BSM/C5GM1/Chol 50:20:10:20 mol/mol/mol/mol) 1:10 molar ratio; protein/BODIPY FL C5-GM1 1:1 (Sup35-C5GM1-Fs)).

When needed, preamyloid Sup35 assemblies were collected 0–1 h after dialysis and used for the preparation of confocal samples.

TEM analysis

Protein aggregates were examined by TEM after adsorption onto formvar/carbon-coated 400 mesh nickel grids (Agar Scientific, Stansted, UK) and negative staining with 2.0% (w/v) uranyl acetate (Sigma-Aldrich, Saint Louis, MO). The grids were observed in a JEM 1010 (80 kV) transmission electron microscope (JEOL, Tokyo, Japan). FFT frequency spectra were obtained by using Fiji software on TEM images from areas of 3.37 × 3.37 μm size (1024 × 1024 pixels, 3.29 × 3.29 nm pixel size). Average linear plots were obtained from three different FFT spectra from each experimental protocol. In each FFT spectrum, 30 linear plots (5° rotation) were obtained and averaged. The first derivative was applied to each averaged linear plot (dy/dx, dx = 22 pixels), and values nearest to 0 or corresponding to 0 in the first derivative were considered correspondent to the peak of the linear plot. A threshold-based bandpass filtering method was applied on FFT frequency spectra obtained from regions of interest (~421 × 421 nm, 128 × 128 pixels) containing fibril assemblies to perform a more accurate analysis of their structures. In each frequency spectrum, a threshold value was set to filter about the 98.5% of the total frequencies. After removing the low-frequency peak from the remaining 1.5%, an inverse FFT was performed to identify the spatial components corresponding to the remaining peaks. In each inverse FFT, a region of interest containing one representative fibril was then selected and analyzed by FFT to get further insight on the structural motifs of its spatial components. A low bandpass filter was applied to TEM images to remove noise; all frequencies beyond 7 nm/cycle were removed from the frequency spectra, and the corresponding inverse FFTs were used.

ANS fluorescence

Samples containing aggregating Sup35 at 10 μM concentration in the presence of a GM1-containing lipid dispersion were investigated for their ability to bind 8-anilinonaphthalene-1-sulfonic acid (ANS; Sigma-Aldrich). Briefly, 50 μL of the protein in assembly buffer were mixed with 450 μL of a solution containing 55 μM ANS in phosphate-buffered saline (PBS). Then, the fluorescence spectra were recorded in the 400–600 nm range in a 2 × 10 mm quartz cuvette using a Perkin-Elmer LS 55 spectrofluorometer (Waltham, MA) equipped with a thermostated cell holder attached to a Haake F8 water bath (Karlsruhe, Germany). The excitation wavelength was 350 nm. The data were analyzed by subtracting blank spectra consisting of the dye dissolved in PBS in the absence of protein.

Cell culture and cell viability assay

Murine endothelioma H-END cells were kindly provided by Prof. F. Bussolino (University of Turin, Italy) and cultured in Dulbecco's modified Eagle's medium containing fetal bovine serum (10%), glutamine (3.0 mM), penicillin (100 units/mL), and streptomycin (100 μg/mL) in a 5.0% CO_2 humidified atmosphere at 37°C. All materials used for cell culture were from Sigma-Aldrich.

The toxicity of the different forms of Sup35 aggregates was assessed by the 3-(4,5-dimethylthiazol-2-yl)-2,5-diphenyltetrazolium bromide (MTT) reduction inhibition assay (40), in which MTT, a yellow redox dye, is reduced to purple formazan by the metabolically active cells. Briefly, the cells were plated at a density of 1500 cells/well on 96-well plates in culture medium (100 μL). After 48 h, the medium was changed with 100 μL of fresh medium supplemented with 10 μL of assembly buffer alone or containing increasing concentrations of the different Sup35 aggregates or intermediate species, and the cells were then incubated for different times. After this treatment, the cells were incubated for 2 h with serum-free Dulbecco's modified Eagle's medium (100 μL) without phenol red, containing MTT (0.5 mg/mL). Then, 100 μL of cell lysis solution (20% SDS, 50% N, N-dimethylformamide) was added to each well, and the samples were incubated at 37°C to allow complete lysis. The blue formazan absorbance values were measured at 595 nm with an automatic plate reader (Bio-Rad, Hercules, CA).

Confocal immunofluorescence

Subconfluent H-END cells grown on glass coverslips in 12-well plates were treated for different times (3, 24, 48, 72 h) with the diverse forms of Sup35 (Sup35-Fs, 1:1 Sup35-GM1-Fs, Sup35-C5GM1-Fs) or preamyloid Sup35 assemblies; 720 μL culture medium was implemented with 80 μL assembly buffer alone or with Sup35 (1 μM final concentration). After incubation, the cells were washed with PBS and fixed in 2.0% buffered paraformaldehyde for 10 min. Cell surface GM1 labeling was performed by incubating the cells with 10 ng/mL cholera toxin, subunit B Alexa488 (Molecular Probes, Eugene, OR) in complete medium for 20 min at room temperature. After counterstaining, the cells were incubated 1 h at room temperature with a rabbit polyclonal antibody raised against full-length Sup35 (Proteintech group, Manchester, UK) diluted 1:5000 in the blocking solution and then washed with PBS for 30 min under stirring. The immunoreaction was revealed with Alexa568-conjugated anti-rabbit secondary antibody (Molecular Probes) diluted 1:400 in PBS. Finally, the cells were washed twice in

PBS and once in redistilled water to remove any nonspecifically bound antibody.

Cell fluorescence was visualized using a confocal Leica TCS SP5 scanning microscope (Leica, Mannheim, Germany) equipped with a HeNe/Ar laser source for fluorescence measurements. Observations were performed using a Leica Plan Apo 63× oil immersion objective, suited with optics for differential interference contrast (DIC) acquisition. Series of optical sections (0.2 μm size, 0.3 μm Z-step) were acquired.

Data analysis and statistics

Statistical analysis was performed by means of the Prism program (Graph Pad Software, San Diego, CA) using Student's *t*-test for grouped data or ANOVA, followed by Tukey's multiple comparison test for all other values. A probability value <0.05 was considered significant.

RESULTS

GM1 modifies the structure of Sup35 amyloid fibril and decreases its cytotoxicity

To check for structural modification induced by GM1 on Sup35 fibrils, we compared, by FFT-TEM analysis, the morphological features of Sup35 aggregates obtained after 72 h in vitro incubation of preamyloid Sup35 assemblies (2) (0–1 h after dialysis), alone (Sup35-Fs) or in the presence of GM1-containing lipid dispersions at two lipid/GM1 molar ratios: 99:1 (1:0.1 Sup35-GM1-Fs) or 90:10 (1:1 Sup35-GM1-Fs). The TEM images of Sup35-Fs showed the presence of long filaments characterized by the typical negative staining of amyloid fibrils (i.e., two parallel black lines, Fig. 1, *A* and *D*, *arrows*), together with thinner positively stained protein filaments (Fig. 1, *A* and *D*, *ars*). Negatively stained amyloid fibrils (~20 nm thick) were not abundant in the sample, as confirmed by the absence of a defined annular component in the FFT frequency spectra (Fig. 1 *A*, *insets a1*, *a2*). However, the mean linear plot showed a shoulder emerging from the low-frequency peak around 20 nm/cycle (Fig. 1 *G*). It is known that the size of Sup35 amyloid fibrils may reach ~20 nm (41). Therefore, it can be suggested that the shoulder in the FFT mean plot could be ascribable to spatial components of double-stained Sup35-Fs in the TEM images. In the 1:0.1 Sup35-GM1-Fs sample (Fig. 1, *B* and *E*), the positively staining feature was almost absent, and the negatively stained fibrils were short, thick, and arranged in a net-like fashion. The structural alterations induced by GM1 were confirmed by a well-defined ring in the FFT spectrum (Fig. 1 *B*, *insets b1*, *b2*), suggesting a higher structural uniformity in amyloid fibrils grown from GM1-interacting oligomers. Moreover, the mean peak of the spectral component in the 1:0.1 Sup35-GM1-Fs sample was found at ~28 nm (Fig. 1 *G*), indicating that the presence of GM1 in the aggregation medium may also induce alterations in the structure of mature fibrils. Such structural modifications were emphasized in the 1:1 Sup35-GM1-Fs sample, in which frequently paired fibrils, longer than the previous sample, were present (Fig. 1, *C* and *F*). The FFT frequency spectra of these fibrils displayed a more defined spectral component (Fig. 1 *C*, *insets c2*, *c3*), and the linear plot showed a peak at ~34 nm (Fig. 1 *G*).

A threshold-based bandpass filtering method was applied on the regions of interest containing fibril assemblies to perform a more accurate analysis of their structures (Fig. 1, *D–F*). In the frequency spectrum of 1:1 Sup35-GM1-Fs (Fig. 1 *F*), we found that by eliminating about 98.50% of the total frequencies, the most represented (~1.5%) consisted of a single peak of low frequencies and heterogenous peaks scattered in the 20–90 nm/cycle range (Fig. 1 *F*, *inset f1*). The spatial components corresponding to these latter peaks, obtained by inverse FFT, were localized mostly on fibrillar structures and showed a scaled shape (Fig. 1 *F*, *inset f2*). By performing FFT on one such spatial component, we obtained a frequency spectrum showing discrete peaks lined up in a regular pattern, consistent with helical coil structure (Fig. 1 *F*, *inset f3*). When the bandpass filter was applied on frequency spectra of Sup35Fs, the filtered domains consisted of a large peak of low frequencies and scant frequency spots (Fig. 1 *D*, *inset d1*). The corresponding spatial components were not associated with fibrillar structures (Fig. 1 *D*, *inset d2*), probably because of a lesser uniformity of Sup35-Fs structure in these samples. The bandpass filter on the frequency spectrum of 1:0.1 Sup35-GM1-Fs identified a relatively small peak of low frequencies and two peaks surrounded by several, scattered frequency spots (Fig. 1 *E*, *inset e1*) at higher frequencies. Inverse FFT of the selected frequencies revealed that some frequency domains corresponded to fibril-associated spatial components (Fig. 1 *E*, *inset e2*). The frequency spectrum obtained from the fibril-associated spatial component showed a straight-line pattern, typical of straight structures, with two peaks corresponding to the ones from the original image (Fig. 1 *E*, *inset e3*). We also tried to assess whether the presence of GM1 during the aggregation process of Sup35 affected the cytotoxicity of aggregation intermediates or mature fibrils. Therefore, we performed the MTT assay on H-END cells exposed for 24 h to Sup35-Fs, 1:0.1 Sup35-GM1-Fs, or 1:1 Sup35-GM1-Fs. As previously reported (2), the amyloid species of Sup35 were per se characterized by a significant cytotoxicity (Fig. 1 *H*), whereas the viability of H-END cells exposed to 1:0.1 Sup35-GM1-Fs or 1:1 Sup35-GM1-Fs was superposable to that of control cells.

GM1 modifies the surface properties of Sup35 fibrils

To assess a possible molecular interaction of GM1 with Sup35 during aggregation, we performed a confocal sensitized FRET analysis of Sup35 fibrils grown in the presence of a lipid dispersion containing a fluorescent GM1 (Sup35-C5GM1-Fs). H-END cells were exposed to

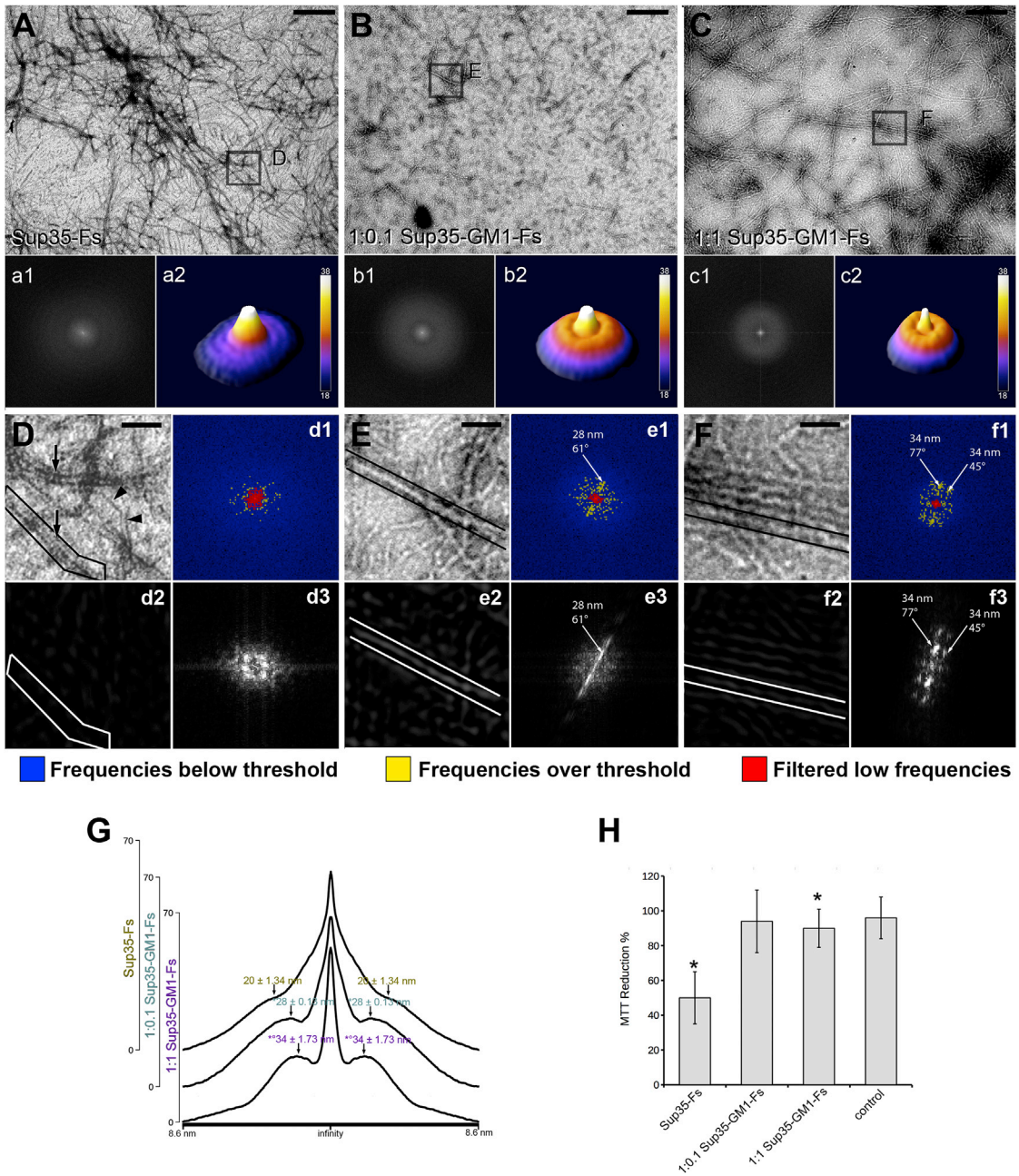

FIGURE 1 TEM and FFT analysis of Sup35 fibrils grown in the absence or in the presence of GM1. (*A–C*) Representative TEM images of Sup35 fibrils grown alone (Sup35-Fs) (*A*) or with a lipid dispersion containing GM1 at 1:0.1 (1:0.1 Sup35-GM1-Fs) (*B*) or 1:1 (1:1 Sup35-GM1-Fs) (*C*) lipid:GM1 molar ratio are shown. Insets (*a1*), (*b1*), (*c1*): two-dimensional frequency spectra of the associated TEM image. Insets (*a2*), (*b2*), (*c2*): three-dimensional surface plots of the related frequency spectra. (*D* and *E*) Magnified details of the corresponding area selected in (*A*) (*D*), (*B*) (*E*), and (*C*) (*F*) are shown; arrows and ars in (*D*) indicate negatively and positively stained fibrils, respectively. Insets (*d1*), (*e1*), (*f1*): FFT frequency spectra of the associated TEM image; the three-color lookup table shows the frequencies that were filtered by the threshold bandpass filter (*blue*), the unfiltered frequencies (*yellow*), and the filtered low-frequency peak (*red*); arrow points at the peak in the FFT. Insets (*d2*), (*e2*), (*f2*): inverse FFT transform of the unfiltered frequencies in (*d1*) (*d2*), (*e1*) (*e2*), and (*f1*) (*f2*). Insets (*d3*), (*e3*), (*f3*): FFT transform of the spatial component selected in (*d2*) (*d3*), (*e2*) (*e3*), and (*f2*) (*f3*). (*G*) Mean linear plots of corresponding FFTs (*a1*, *b1*, *c1*) indicating the spatial frequency of each peak are given (one-way ANOVA, $F_{(2,\ 6)} = 30.422$; $^{*}p < 0.05$ vs. Sup35-Fs, $^{\circ}p < 0.05$ vs. 1:0.1 Sup35-GM1-Fs). (*H*) Cell viability of H-END cells exposed for 24 h to Sup35-Fs, 1:0.1 Sup35-GM1-Fs, or 1:1 Sup35-GM1-Fs are given. Cell viability was checked by the MTT assay (one-way ANOVA $F_{3,8} = 8.3$; $^{*}p < 0.05$ vs. control, n = 3). Values are the average ± standard error (SE) of three independent experiments. Scale bars (*A–C*), 560 nm; insets (*a1*), (*b1*), (*c1*), 188 nm. To see this figure in color, go online.

Sup35-C5GM1-Fs (monomer concentration = 1.0 μM) and immunolabeled with anti-Sup35 antibodies. Confocal analysis revealed a sporadic presence on the cell substrate of small immunostained aggregates displaying the GM1 fluorescence signal (Fig. 2, *A–C*). These aggregates also displayed a strong FRET interaction between C5 fluorochrome on GM1 and Alexa568 on Sup35 fibrils (Fig. 2, *C* and *E*), supporting a close interplay between Sup35 aggregates and GM1 in the lipid dispersion. We also performed ANS experiments to compare the surface properties of Sup35 aggregates grown in the absence or in the presence of GM1. We found a reduced fluorescence intensity of ANS bound to Sup35-GM1-Fs and Sup35-SA-Fs with respect to Sup35-Fs (Fig. 2 *F*), suggesting that the GM1-Sup35 interaction affects surface properties of the fibrils, either increasing their anionic charge and/or reducing their hydrophobicity.

Sup35 fibrils bind differently to cell surfaces when grown in the absence or in the presence of GM1

Once we assessed the close interaction between preamyloid Sup35 assemblies and GM1 during aggregation, we verified whether Sup35-Fs and Sup35-GM1-Fs differently interacted with GM1 on cell membrane (Fig. 3). Fluorescence intensity of GM1 on cell membranes was significantly lower in cells exposed to Sup35-Fs than in cells exposed to Sup35-GM1-Fs and control cells (Fig. 3, *A–C* and *F*). Sup35-Fs on H-END cells appeared as linear or loop-shaped rods, establishing remarkable interactions with GM1 in the plasma membrane (Fig. 3 *C*). In detail, clusters of GM1 fluorescence were frequently observed adjacent to Sup35-Fs (*inset* in Fig. 3 *C*). Accordingly, an intense FRET interaction between GM1 staining (Alexa488-conjugated cholera toxin, subunit B) and Sup35 immunolabeling (Alexa568) was observed (Fig. 3, *D* and *E*). Sup35-GM1-Fs interacting with GM1 were rarely found in the plasma membrane (Fig. 3 *F* and *inset*); consequently, GM1 signal distribution on the cell membrane was unaffected. Moreover, FRET efficiency between Alexa488 and Alexa568 was negligible on Sup35-GM1-Fs (Fig. 3, *G* and *H*). In line with these data, our confocal analyses revealed that the overlap coefficient between the two fluorochromes was significantly lower in these fibrils than in Sup35-Fs (Table 1).

Sup35 aggregation involves GM1 in the cell membrane and induces cell damage

We next assessed Sup35 aggregation on cell surface. H-END cells were exposed to preamyloid Sup35 assemblies (2) (0–1 h after dialysis, 1.0 μM monomer concentration) for 24, 48, or 72 h (int-24, 48, 72), and the structural features and cytotoxicity of the resulting aggregates were compared with those of Sup35 fibrils grown in batch in the absence of

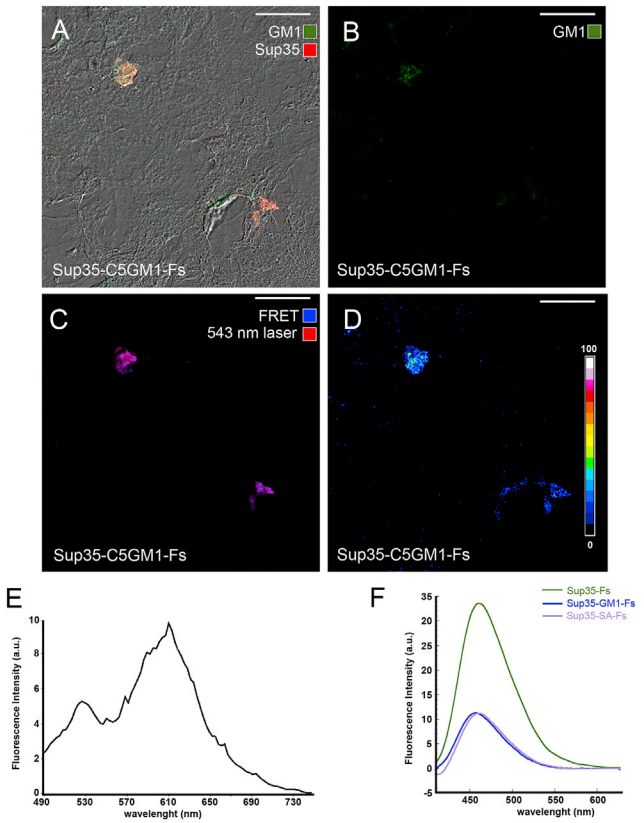

FIGURE 2 GM1 binds to aggregating fibrils and modifies their surface properties. (*A–E*) Sup35-GM1-Fs were grown by incubating Sup35 preamyloid species with a lipid dispersion containing fluorescent GM1 (BODIPY FL C5-GM1, Sup35-C5GM1-Fs; *green*) and seeded on an H-END cell substrate for 3 h. Then, the aggregates were stained (Alexa568, *red*) and analyzed by confocal microscopy. (*A*) Maximal intensity Z-projections of the two fluorescence signals merged with DIC images of H-END cells are shown. (*B* and *C*) Green (*B*, Alexa488), and merged channels of Alexa568 fluorescence (*C*), excited with the 543 nm laser line (*red*) or by FRET (*blue*), are shown. (*D*) shows a significant efficiency of FRET interaction between the two fluorochromes. (*E*) Spectral analysis of fluorescence emission excited by the 458 nm laser line performed on seeded aggregates is shown; the 610 nm peak indicates the presence of FRET interaction between BODIPY FL C5 on GM1 and Alexa568 on Sup35. (*F*) ANS binding to Sup35-Fs, Sup35-GM1-Fs, and Sup35-SA-Fs is shown. Scale bars, 24 μm. To see this figure in color, go online.

GM1 and administered to H-END cells for the same times (Sup35-Fs-24, 48, 72). Morphological and quantitative analyses revealed a time of exposure-dependent Sup35-Fs size increase (Fig. 4, *A–C* and *G*). Exposure of H-END cells for 48 h to preamyloid Sup35 assemblies led to the formation of aggregates, the size of which increased with time. In comparison, the average size of Sup35-Fs-24, Sup35-Fs-48, and Sup35-Fs-72 deposits remained unchanged with time (Fig. 4, *D–G*). A strong FRET signal and a high overlap coefficient were found in all the specimens analyzed (*insets* in Fig. 4, *A–F*; Table 1), indicating that Sup35 fibrils either formed on cell membrane or assembled in vitro both established molecular interactions with GM1. Fig. 4 *H* shows a significant reduction of viability of cells exposed for 24 h

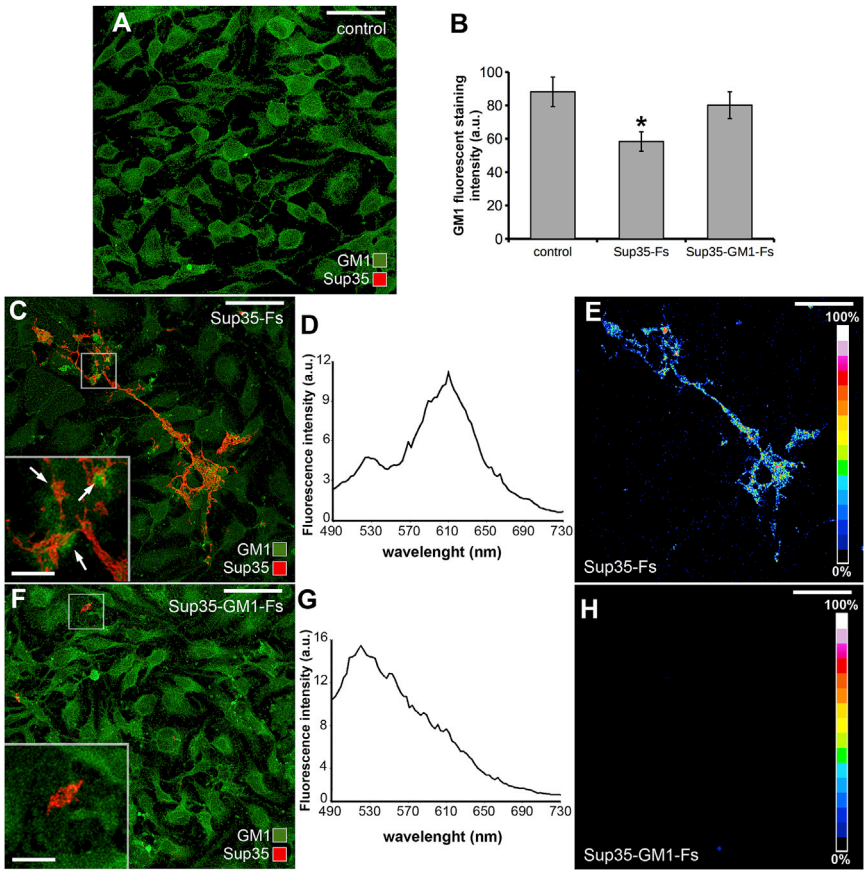

FIGURE 3 Interactions between Sup35-Fs or Sup35-GM1-Fs and GM1 in the H-END plasma membrane. Sup35-Fs and Sup35-GM1-Fs (*red*) were seeded (24 h) on an H-END cell substrate, and GM1 was revealed in the cell membrane with Alexa488-conjugated cholera toxin (CT-X; *green*). (*A*) Representative images of untreated control cells are shown. (*B*) Quantitative analysis of fluorescence intensity of GM1 staining on control, Sup35-Fs-, and Sup35-GM1-Fs-treated H-END cells is shown (one-way ANOVA $F_{(2,\ 6)} = 14.86$, $^*p < 0.05$ vs. control, n = 3). Values are the average ± standard error (SE) of three independent experiments. (*C–E*) Confocal image (*C*), emission spectrum (*D*), and FRET efficiency analysis (*E*) of Sup35-Fs seeded on H-END cells are shown. (*F–H*) Confocal image (*F*), emission spectrum (*G*), and FRET efficiency analysis (*H*) of Sup35-GM1-Fs seeded on H-END cells are shown. Insets in (*C*) and (*F*) show magnified details of the selected areas; arrows indicate GM1 clusters adjacent to Sup35 aggregates. Scale bars (*A*, *C*, *E*, *F*, and *H*), 40 μm; insets, 8 μm. To see this figure in color, go online.

to both preamyloid Sup35 and Sup35-Fs compared to untreated cells. The viability of cells exposed 24, 48, and 72 h to Sup35-Fs was unaffected, whereas that of cells exposed to preamyloid Sup35 significantly decreased after 48 and 72 h. These data suggest a direct link between preamyloid Sup35 interaction with plasma membrane GM1 in the fibrillation path and cell damage.

DISCUSSION

Aggregation into amyloid assemblies of proteins and peptides both in denatured or native form requires the establishment of intra- or interchain hydrophobic and electrostatic interactions (42). Such processes are affected by the presence of many molecules, particularly amphipathic ones, whose binding with amyloid species inhibits, promotes, or redirects the fibrillation process (13). A large wealth of coherent data indicates that the amphipathic molecule of plasma membrane GM1 is involved in amyloid nucleation, growth, and cytotoxicity by interacting with monomeric, oligomeric, or fibrillar species of peptides and proteins (2,43–47). In this study, we investigated the effects of nonspecific interactions between GM1 and diverse amyloid species of a yeast prion protein (Sup35), both in aggregation medium and in cultured cells, in terms of structural features and cytotoxicity of the resulting amyloid assemblies.

TABLE 1 Colocalization Analysis of Plasma Membrane GM1 and Different Species of Sup35

	24 h	48 h	72 h
1:1 Sup35-GM1-Fs	0.267 ± 0.017	–	–
Sup35-Fs	0.768 ± 0.015*	0.723 ± 0.025*	0.731 ± 0.036*
Intermediate species	0.653 ± 0.011*	0.684 ± 0.007*	0.706 ± 0.008*

One-way ANOVA $F_{(6,\ 14)} = 78.92$. Data are reported as mean ± SE.
$^*p < 0.01$ vs. 1:1 Sup35-GM1-Fs, n = 3.

We report that two different yeast prion Sup35 fibrillar assemblies generated under different aggregation conditions display different cytotoxicity. Toxic fibrils were obtained when Sup35 was aggregated in the absence of GM1, whereas nontoxic fibrils were generated in the presence of GM1. Previous studies demonstrated that GM1-containing lipid dispersions may consist of double-layer liposomes and rich micelles, and such a coexistence of highly charged micelles and membrane with low surface-charge density may have a different impact on the interaction, nucleation, and aggregation process (48). Nevertheless, our data suggest that the interactions between amphipathic molecules, such as GM1, and amyloid precursors during the fibrillation process may alter the biophysical properties of the resulting

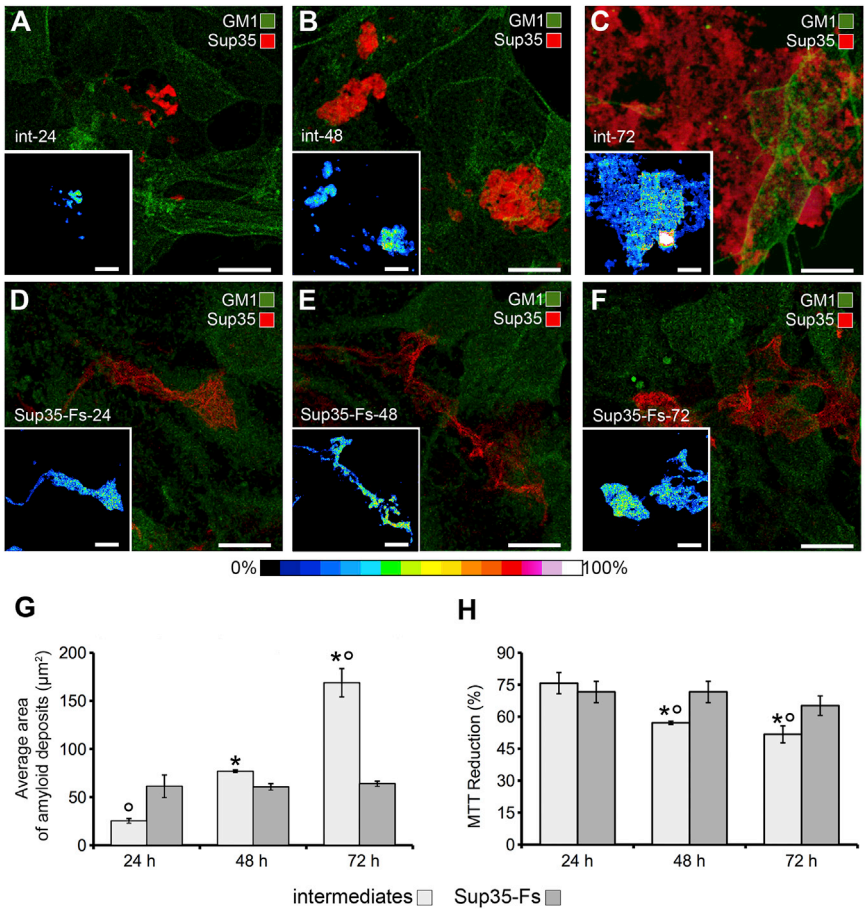

FIGURE 4 Sup35 aggregation is promoted by the cell membrane. (*A–F*) Confocal images and FRET analysis of preamyloid Sup35 intermediates (*red*) grown on the H-END cell membrane for 24 h (int-24, *A*), 48 h (int-48, *B*), or 72 h (int-72, *C*) or fibrils aggregated in batch for 72 h and then administered to H-END cells for 24 h (Sup35-Fs-24, *D*), 48 h (Sup35-Fs-48, *E*), or 72 h (Sup35-Fs-48, *F*); cell membrane GM1 was revealed by Alexa488-conjugated CT-X staining (*green*); insets show the efficiency of sensitized FRET between Alexa568 conjugated to anti-Sup35 antibodies and Alexa488 conjugated to CT-X. (*G*) Quantitative analysis of the average area of Sup35 aggregates in the previous experimental conditions (one-way ANOVA, $F_{(2,\ 6)} = 13.62$, $^{*}p < 0.05$ vs. 24 h, n = 3; *t*-test, $^{\circ}p < 0.05$ vs. fibrils, n = 3); (*H*) Cytotoxicity of the same samples performed by the MTT assay on H-END cells is shown (one-way ANOVA, $F_{(2,\ 6)} = 8.75$, $^{*}p < 0.05$ vs. 24 h, n = 3; *t*-test, $^{\circ}p < 0.05$ vs. fibrils n = 3); values were converted into percentage of control (control = 100%) and expressed as average ± SE. Scale bars, 10 μm. To see this figure in color, go online.

amyloid fibrils. Amyloid oligomer or fibril toxicity can be rationalized by a function combining oligomer and fibril properties such as size and extent of hydrophobic surface (49). Reduced surface hydrophobicity in Sup35 fibrils grown in the presence of GM1-containing lipid dispersions could, indeed, explain their reduced interaction with the cell membrane and, more specifically, with GM1-enriched microdomains on the plasma membrane. Moreover, the saturation of the hydrophobic and hydrophilic sites of Sup35 by anionic GM1 may parallel and enhance this effect.

TEM and FFT analysis revealed that Sup35-GM1-Fs displayed higher structural uniformity than Sup35-Fs, indicating that the reduction of aggregate cytotoxicity by GM1 was associated with a more ordered fibrillar structure also involving fibril solvation by GM1. It also has to be considered that the assembly buffer contained high concentrations of small molecules such as Tris, NaCl, and glycerol. These molecules could determine chemical properties of the buffer such as high pH and ionic strength and a disordered bulk phase of water that could either hinder (50) or favor (51) GM1 interactions with the amyloid peptide. Therefore, it is uncertain whether the dependence of the structural changes of Sup35 fibrils on lipid concentration could be precisely reproduced in vivo. However, it is reasonable to assume that the different structural organization of toxic and nontoxic Sup35 fibrils most likely resulted from a direct interaction of GM1 with the fibril precursors. Accordingly, confocal FRET analysis of Sup35 fibrils grown in the presence of fluorescently labeled GM1 molecules revealed their binding to the fibrillar assemblies. Similarly, ANS analysis indicated either higher negative charge and/or lower hydrophobicity in Sup35-GM1-Fs surfaces than in Sup35-Fs. This effect recalls a recent study showing that toxic oligomers of a bacterial protein, HyPF-N, differed from their nontoxic counterparts in several properties, including the exposure of a higher number of hydrophobic residues (52). Actually, the differences we report could be due either to the nonspecific binding of GM1 to the Sup35 fibril precursors and/or to the interaction and solvation process by anionic GM1 of Sup35 mature fibrils. Accordingly, FRET and confocal analyses on fibril-membrane interaction revealed a low affinity of Sup35-GM1-Fs with the plasma membrane, suggesting that a reduced capacity to remove membrane GM1 and possibly other charged regulatory lipids from H-END cells may underlay their low cytotoxicity. This hypothesis is supported by the known detrimental effects of anionic lipid reduction in neurodegenerative diseases such as Parkinson's and Alzheimer's diseases (53,54). The same process may

account for the interference of synthetic or natural amphipathic molecules and plant polyphenols such as resveratrol, curcumin, and oleuropein aglycone with amyloid toxicity (55,56). In fact, these molecules are able to affect the interaction of amyloid peptides with cell membrane components (57,58). Our ANS data suggest that either repulsive forces between negative charges and/or saturation of anionic and hydrophobic sites of Sup35 by Gm1 may underlie such reduced capacity. In this view, net-like arrangement of 1:0.1 Sup35-GM1-Fs in TEM images may minimize fibril-fibril contacts, thus suggesting ionic repulsion. On the other hand, these forces do not appear remarkable in 1:1 Sup35-GM1-Fs, in which fibrils were frequently contiguous to each other. We hypothesize that different structural features of amyloid fibrils may affect fibril-fibril and possibly cell-fibril interactions, depending on the extent of the interplay between amphipathic molecules and amyloid precursors during the aggregation process.

Most researchers agree that both oligomeric and fibrillar aggregates can exert amyloid cytotoxicity by interacting with cell membrane components (59–61). Our data confirm that the medium composition heavily affects the structural features of amyloid aggregates and the degree of their cytotoxicity by modifying either the physicochemical interactions in the aggregation path or the surface properties of amyloid fibrils. Indeed, fibrillar aggregates grown in vitro remarkably differ from that grown in vivo either because different fibril precursors are generated after their interactions or not with molecules in different environments or because the resulting fibrils are naked, in one case, or covered by molecules they bind, such as GM1, in the second case.

It has been reported that oligomer toxicity emerges not only from their intrinsic biophysical properties but also from the biochemical features of the lipid membrane they interact with. In this sense, the increased or reduced presence of GM1 in the cell membrane modulates the interaction of preformed oligomers with the membrane itself, increasing or reducing their toxic properties, respectively (2,24–29). Data in this study suggest that such interactions may promote amyloid fibrillation onto the cells, thus inducing cytotoxic effects. Taking into consideration that fibrillar aggregation is a ubiquitous process reported in vivo in amyloid diseases, it is reasonable to assume that fibrillation cytotoxicity may parallel the intrinsic oligomer toxicity.

In conclusion, our data suggest that in vivo amyloid fibrillation imply monomer-oligomer interactions with membrane components, such as anionic lipids, that may be nonspecific and mediated by covalent, noncovalent, ionic, or hydrophobic bonds. On the one hand, such interactions can induce cell damage; on the other hand, they may affect structural and/or surface features of fibrillation intermediates and reduce the cytotoxicity of the final fibrillar products.

Further studies on the molecular processes occurring between the species arising during amyloid fibrillation and plasma membrane components of cells are needed to gain better insight into the molecular basis of amyloid cytotoxicity toward different cell/tissues. This will prove useful to design new molecular scaffolds and therapeutic strategies against amyloid diseases.

AUTHOR CONTRIBUTIONS

M.B.: conception and design, collection and assembly of data, data analysis and interpretation, TEM, confocal immunofluorescence, manuscript writing, financial support. M.L.: collection and assembly of data, LUV preparation, ANS assay, cell culture and cell viability assay. M.S.: revising of manuscript. M.R.: Sup35 production and assembly, revising the manuscript. S.Z.-O.: revising of manuscript. D.N.: conception and design, collection and assembly of data, data analysis and interpretation, TEM, FFT analyses, confocal immunofluorescence, manuscript writing, financial support.

ACKNOWLEDGMENTS

We thank Dr. Ugo Santosuosso, University of Florence, for his assistance in the FFT analyses.

This work was supported by Ente Cassa di Risparmio di Firenze (No. 2015.1002A2202.3931). M.L. was supported by ANCC-COOP/Airalzh ONLUS (Reg. no. 0043966.30-10- 359 2014-u) through the University of Florence (D.R.595/2016).

REFERENCES

1. M'bappé, P., and G. Grateau. 2012. Osteo-articular manifestations of amyloidosis. *Best Pract. Res. Clin. Rheumatol.* 26:459–475.
2. Bucciantini, M., D. Nosi, …, M. Stefani. 2012. Toxic effects of amyloid fibrils on cell membranes: the importance of ganglioside GM1. *FASEB J.* 26:818–831.
3. Eisenberg, D., and M. Jucker. 2012. The amyloid state of proteins in human diseases. *Cell.* 148:1188–1203.
4. Khondker, A., R. J. Alsop, and M. C. Rheinstädter. 2017. Membrane-accelerated amyloid-β aggregation and formation of cross-β sheets. *Membranes (Basel).* 7:49.
5. Pellistri, F., M. Bucciantini, …, M. Stefani. 2008. Nonspecific interaction of prefibrillar amyloid aggregates with glutamatergic receptors results in Ca^{2+} increase in primary neuronal cells. *J. Biol. Chem.* 283:29950–29960.
6. De Felice, F. G., P. T. Velasco, …, W. L. Klein. 2007. Abeta oligomers induce neuronal oxidative stress through an N-methyl-D-aspartate receptor-dependent mechanism that is blocked by the Alzheimer drug memantine. *J. Biol. Chem.* 282:11590–11601.
7. Hou, X., H. C. Parkington, …, D. H. Small. 2007. Transthyretin oligomers induce calcium influx via voltage-gated calcium channels. *J. Neurochem.* 100:446–457.
8. Pannuzzo, M., A. Raudino, …, M. Karttunen. 2013. α-helical structures drive early stages of self-assembly of amyloidogenic amyloid polypeptide aggregate formation in membranes. *Sci. Rep.* 3:2781.
9. Shrivastava, A. N., A. Aperia, …, A. Triller. 2017. Physico-pathologic mechanisms involved in neurodegeneration: misfolded protein-plasma membrane interactions. *Neuron.* 95:33–50.
10. Stefani, M., and S. Rigacci. 2013. Protein folding and aggregation into amyloid: the interference by natural phenolic compounds. *Int. J. Mol. Sci.* 14:12411–12457.
11. Canale, C., R. Oropesa-Nuñez, …, S. Dante. 2018. Amyloid and membrane complexity: the toxic interplay revealed by AFM. *Semin. Cell Dev. Biol.* 73:82–94.

12. Leri, M., F. Bemporad, …, M. Bucciantini. 2016. Molecular insights into cell toxicity of a novel familial amyloidogenic variant of β2-microglobulin. *J. Cell. Mol. Med.* 20:1443–1456.
13. Penke, B., G. Paragi, …, L. VÍgh. 2018. The role of lipids and membranes in the pathogenesis of Alzheimer's disease: a comprehensive view. *Curr. Alzheimer Res.* 15:1191–1212.
14. Bucciantini, M., S. Rigacci, and M. Stefani. 2014. Amyloid aggregation: role of biological membranes and the aggregate-membrane system. *J. Phys. Chem. Lett.* 5:517–527.
15. Ladiwala, A. R., M. Mora-Pale, …, P. M. Tessier. 2011. Polyphenolic glycosides and aglycones utilize opposing pathways to selectively remodel and inactivate toxic oligomers of amyloid β. *ChemBioChem.* 12:1749–1758.
16. Ryan, T. M., A. Friedhuber, …, B. R. Roberts. 2012. Small amphipathic molecules modulate secondary structure and amyloid fibril-forming kinetics of Alzheimer disease peptide Aβ(1-42). *J. Biol. Chem.* 287:16947–16954.
17. Assarsson, A., E. Hellstrand, …, S. Linse. 2014. Charge dependent retardation of amyloid β aggregation by hydrophilic proteins. *ACS Chem. Neurosci.* 5:266–274.
18. Pellistri, F., M. Bucciantini, …, M. Stefani. 2013. Different ataxin-3 amyloid aggregates induce intracellular Ca(2+) deregulation by different mechanisms in cerebellar granule cells. *Biochim. Biophys. Acta.* 1833:3155–3165.
19. Monteiro, F. A., I. Cardoso, …, M. J. Saraiva. 2006. In vitro inhibition of transthyretin aggregate-induced cytotoxicity by full and peptide derived forms of the soluble receptor for advanced glycation end products (RAGE). *FEBS Lett.* 580:3451–3456.
20. Kam, T. I., S. Song, …, Y. K. Jung. 2013. FcγRIIb mediates amyloid-β neurotoxicity and memory impairment in Alzheimer's disease. *J. Clin. Invest.* 123:2791–2802.
21. Yanagisawa, K. 2015. GM1 ganglioside and Alzheimer's disease. *Glycoconj. J.* 32:87–91.
22. Yamamoto, N., T. Matsubara, …, K. Yanagisawa. 2008. Age-dependent high-density clustering of GM1 ganglioside at presynaptic neuritic terminals promotes amyloid beta-protein fibrillogenesis. *Biochim. Biophys. Acta.* 1778:2717–2726.
23. Matsuzaki, K. 2014. How do membranes initiate Alzheimer's Disease? Formation of toxic amyloid fibrils by the amyloid β-protein on ganglioside clusters. *Acc. Chem. Res.* 47:2397–2404.
24. Sasahara, K., K. Morigaki, and K. Shinya. 2013. Effects of membrane interaction and aggregation of amyloid β-peptide on lipid mobility and membrane domain structure. *Phys. Chem. Chem. Phys.* 15:8929–8939.
25. Evangelisti, E., R. Cascella, …, C. Cecchi. 2016. Binding affinity of amyloid oligomers to cellular membranes is a generic indicator of cellular dysfunction in protein misfolding diseases. *Sci. Rep.* 6:32721.
26. Calamai, M., E. Evangelisti, …, F. Pavone. 2016. Single molecule experiments emphasize GM1 as a key player of the different cytotoxicity of structurally distinct $A\beta_{1\text{-}42}$ oligomers. *Biochim. Biophys. Acta.* 1858:386–392.
27. Calamai, M., and F. S. Pavone. 2013. Partitioning and confinement of GM1 ganglioside induced by amyloid aggregates. *FEBS Lett.* 587:1385–1391.
28. Calamai, M., and F. S. Pavone. 2011. Single molecule tracking analysis reveals that the surface mobility of amyloid oligomers is driven by their conformational structure. *J. Am. Chem. Soc.* 133:12001–12008.
29. Yahi, N., A. Aulas, and J. Fantini. 2010. How cholesterol constrains glycolipid conformation for optimal recognition of Alzheimer's beta amyloid peptide (Abeta1-40). *PLoS One.* 5:e9079.
30. Malchiodi-Albedi, F., V. Contrusciere, …, M. Diociaiuti. 2010. Lipid raft disruption protects mature neurons against amyloid oligomer toxicity. *Biochim. Biophys. Acta.* 1802:406–415.
31. Hong, S., B. L. Ostaszewski, …, D. J. Selkoe. 2014. Soluble Aβ oligomers are rapidly sequestered from brain ISF in vivo and bind GM1 ganglioside on cellular membranes. *Neuron.* 82:308–319.
32. Sokolova, T. V., I. O. Zakharova, …, N. F. Avrova. 2007. Neuroprotective effect of ganglioside GM1 on the cytotoxic action of hydrogen peroxide and amyloid beta-peptide in PC12 cells. *Neurochem. Res.* 32:1302–1313.
33. Maglione, V., P. Marchi, …, S. Sipione. 2010. Impaired ganglioside metabolism in Huntington's disease and neuroprotective role of GM1. *J. Neurosci.* 30:4072–4080.
34. Krzewska, J., and R. Melki. 2006. Molecular chaperones and the assembly of the prion Sup35p, an in vitro study. *EMBO J.* 25:822–833.
35. Pezza, J. A., J. Villali, …, T. R. Serio. 2014. Amyloid-associated activity contributes to the severity and toxicity of a prion phenotype. *Nat. Commun.* 5:4384.
36. Bracewell, R. 1999. The Fourier Transform & Its Applications, Third Edition. McGraw-Hill, New York.
37. Nosi, D., G. Delfino, and F. Quercioli. 2013. Serous cutaneous glands in anurans: Fourier transform analysis of the repeating secretory granule substructure. *Naturwissenschaften.* 100:209–218.
38. Kong, C., K. Ito, …, H. Song. 2004. Crystal structure and functional analysis of the eukaryotic class II release factor eRF3 from *S. pombe*. *Mol. Cell.* 14:233–245.
39. Krzewska, J., M. Tanaka, …, R. Melki. 2007. Biochemical and functional analysis of the assembly of full-length Sup35p and its prion-forming domain. *J. Biol. Chem.* 282:1679–1686.
40. Mosmann, T. 1983. Rapid colorimetric assay for cellular growth and survival: application to proliferation and cytotoxicity assays. *J. Immunol. Methods.* 65:55–63.
41. Kawai-Noma, S., C. G. Pack, …, A. Hirata. 2010. In vivo evidence for the fibrillar structures of Sup35 prions in yeast cells. *J. Cell Biol.* 190:223–231.
42. Marshall, K. E., K. L. Morris, …, L. C. Serpell. 2011. Hydrophobic, aromatic, and electrostatic interactions play a central role in amyloid fibril formation and stability. *Biochemistry.* 50:2061–2071.
43. Novitskaya, V., N. Makarava, …, I. V. Baskakov. 2007. Amyloid fibrils of mammalian prion protein induce axonal degeneration in NTERA2-derived terminally differentiated neurons. *J. Neurochem.* 102:398–407.
44. Matsubara, T., M. Nishihara, …, T. Sato. 2017. Size and shape of amyloid fibrils induced by ganglioside nanoclusters:role of sialyl oligosaccharide in fibril formation. *Langmuir.* 33:13874–13881.
45. Hoshino, T., M. I. Mahmood, …, K. Matsuzaki. 2013. Binding and aggregation mechanism of amyloid β-peptides onto the GM1 ganglioside-containing lipid membrane. *J. Phys. Chem. B.* 117:8085–8094.
46. Grey, M., C. J. Dunning, …, S. Linse. 2015. Acceleration of α-synuclein aggregation by exosomes. *J. Biol. Chem.* 290:2969–2982.
47. Kakio, A., S. I. Nishimoto, …, K. Matsuzaki. 2001. Cholesterol-dependent formation of GM1 ganglioside-bound amyloid beta-protein, an endogenous seed for Alzheimer amyloid. *J. Biol. Chem.* 276:24985–24990.
48. Mojumdar, E. H., C. Grey, and E. Sparr. 2019. Self-assembly in ganglioside–phospholipid systems: the co-existence of vesicles, micelles, and discs. *Int. J. Mol. Sci.* 21:56.
49. Mannini, B., E. Mulvihill, …, F. Chiti. 2014. Toxicity of protein oligomers is rationalized by a function combining size and surface hydrophobicity. *ACS Chem. Biol.* 9:2309–2317.
50. Chi, E. Y., S. L. Frey, and K. Y. Lee. 2007. Ganglioside G(M1)-mediated amyloid-beta fibrillogenesis and membrane disruption. *Biochemistry.* 46:1913–1924.
51. Bianco, I. D., G. D. Fidelio, and B. Maggio. 1988. Effect of glycerol on the molecular properties of cerebrosides, sulphatides and gangliosides in monolayers. *Biochem. J.* 251:613–616.
52. Capitini, C., J. R. Patel, …, F. Chiti. 2018. Structural differences between toxic and nontoxic HypF-N oligomers. *Chem. Commun. (Camb.).* 54:8637–8640.
53. Wu, G., Z. H. Lu, …, R. W. Ledeen. 2012. Deficiency of ganglioside GM1 correlates with Parkinson's disease in mice and humans. *J. Neurosci. Res.* 90:1997–2008.

54. Berman, D. E., C. Dall'Armi, …, G. Di Paolo. 2008. Oligomeric amyloid-beta peptide disrupts phosphatidylinositol-4,5-bisphosphate metabolism. *Nat. Neurosci.* 11:547–554.

55. Rigacci, S., V. Guidotti, …, M. Stefani. 2011. Aβ(1-42) aggregates into non-toxic amyloid assemblies in the presence of the natural polyphenol oleuropein aglycon. *Curr. Alzheimer Res.* 8:841–852.

56. Khondker, A., R. J. Alsop, …, M. C. Rheinstädter. 2018. Membrane-modulating drugs can affect the size of amyloid-β $_{25-35}$ aggregates in anionic membranes. *Sci. Rep.* 8:12367.

57. Leri, M., D. Nosi, …, M. Bucciantini. 2016. The polyphenol Oleuropein aglycone hinders the growth of toxic transthyretin amyloid assemblies. *J. Nutr. Biochem.* 30:153–166.

58. Leri, M., A. Natalello, …, M. Bucciantini. 2019. Oleuropein aglycone and hydroxytyrosol interfere differently with toxic Aβ_{1-42} aggregation. *Food Chem. Toxicol.* 129:1–12.

59. Canale, C., S. Torrassa, …, A. Gliozzi. 2006. Natively folded HypF-N and its early amyloid aggregates interact with phospholipid monolayers and destabilize supported phospholipid bilayers. *Biophys. J.* 91:4575–4588.

60. Stefani, M. 2010. Biochemical and biophysical features of both oligomer/fibril and cell membrane in amyloid cytotoxicity. *FEBS J.* 277:4602–4613.

61. Rawat, A., R. Langen, and J. Varkey. 2018. Membranes as modulators of amyloid protein misfolding and target of toxicity. *Biochim. Biophys. Acta Biomembr.* 1860:1863–1875.